BCTR: Bidirectional Conditioning Transformer for Scene Graph Generation

Peng Hao[1], Xiaobing Wang[1], Yingying Jiang[1], Hanchao Jia[1], Xiaoshuai Hao[2*]
[1]Samsung R&D Institute China-Beijing
[2]Beijing Academy of Artificial Intelligence
{peng1.hao, x0106.wang, yy.jiang, hanchao.jia}@samsung.com, xshao@baai.ac.cn

Abstract

Scene Graph Generation (SGG) remains a challenging task due to its compositional property. Previous approaches improve prediction efficiency through end-to-end learning. However, these methods exhibit limited performance as they assume unidirectional conditioning between entities and predicates, which restricts effective information interaction. To address this limitation, we propose a novel bidirectional conditioning factorization in a semantic-aligned space for SGG, enabling efficient and generalizable interaction between entities and predicates. Specifically, we introduce an end-to-end scene graph generation model, the Bidirectional Conditioning Transformer (BCTR), to implement this factorization. BCTR consists of two key modules. First, the Bidirectional Conditioning Generator (BCG) performs multi-stage interactive feature augmentation between entities and predicates, enabling mutual enhancement between these predictions. Second, Random Feature Alignment (RFA) is present to regularize feature space by distilling multi-modal knowledge from pre-trained models. Within this regularized feature space, BCG is feasible to capture interaction patterns across diverse relationships during training, and the learned interaction patterns can generalize to unseen but semantically related relationships during inference. Extensive experiments on Visual Genome and Open Image V6 show that BCTR achieves state-of-the-art performance on both benchmarks.

1. Introduction

Scene Graph Generation (SGG) aims to enable computers to understand and interpret images by detecting objects and identifying the relationships between them. This process generates structured relationships in the form of triplets (object-predicate-subject). SGG has significant potential for a wide range of downstream applications, including visual question answering [25], image captioning [32], and text-to-image retrieval [11].

Previous SGG studies can be categorized into two-stage and one-stage approaches. Two-stage methods separate SGG into entity and predicate detection stages, generating $\mathcal{O}(N^2)$ relationship candidates, which demands significant computational resources. Inspired by fully convolutional one-stage object detection [1, 27], one-stage SGG methods detect relationships directly from image features [23, 30], improving detection efficiency by avoiding the considera-

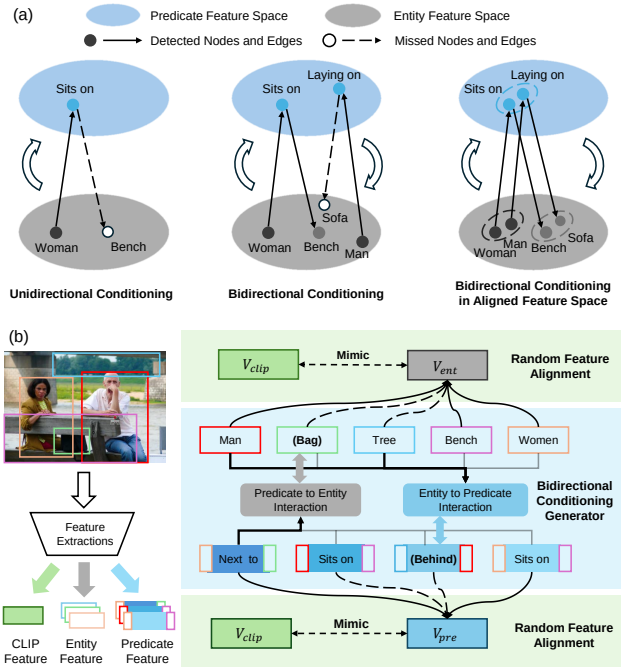

Figure 1. **The motivation and pipeline paradigm of BCTR.** (a) Comparison of different conditioning approaches in SGG. Unlike unidirectional conditioning, bidirectional conditioning can generate relationships through mutual feature augmentation, even when an entity is missing. However, this interaction pattern has limited generalization to unseen categories. The right panel illustrates our approach, which learns bidirectional conditioning within a semantic-aligned space, allowing it to generalize to unseen but semantically related relationships. (b) The left part shows the extraction of CLIP, entity, and predicate features from the input image. The right part demonstrates how BCTR enhances the detection of entities (e.g., "Bag") and predicates (e.g., "Behind") in the semantic-aligned feature space through bidirectional interaction.

*Corresponding author.

tion of all possible pairs. However, these methods lack explicit entity modeling and face challenges with complex relationships within images. To address this, recent one-stage methods [18, 26] condition predicate prediction on entity features to enhance task performance, while their fixed unidirectional dependence often yields suboptimal results, as entity detection does not benefit from predicate information.

To address this limitation, we propose a bidirectional conditioning factorization in a semantic-aligned space for SGG, enabling efficient and generalizable interactions between entities and predicates, as illustrated in Fig. 1 (a). Unlike unidirectional conditioning, bidirectional conditioning can predict correct relationships by leveraging feature interactions to infer missing entity/predicate nodes (e.g., Bench). However, due to the long-tail distribution of the SGG dataset, the learned interactions in an unregularized feature space struggle to generalize to unseen but semantically related relationships (e.g., Man-Laying on-Sofa). The core insight of this paper is that learning bidirectional interaction patterns within a semantic-aligned feature space significantly enhances SGG model performance. The benefits lay in two folds. First, bidirectional interaction learning can be facilitated in the semantic feature space during training. Second, the learned interaction patterns can effectively generalize to unseen relationships during inference.

Motivated by this insight, we propose a one-stage SGG model to implement our factorization, dubbed Bidirectional Conditioning TRansformer (BCTR), as illustrated in Fig. 1 (b). BCTR consists of two core modules: the Bidirectional Conditioning Generator (BCG) and Random Feature Alignment (RFA). The BCG module establishes mutual dependencies between the entity and predicate decoders through two feature interaction mechanisms. The inner interaction utilizes Bidirectional Attention (BiAtt) to enhance information exchange between entities and predicates, while the outer interaction applies iterative refinement to condition current detections on previous estimates, thus improving interactions between predictions. The RFA module is designed to support BCG in learning interaction patterns within a semantic-aligned feature space. By feature distillation with Vision-Language Pre-trained Models (VLPMs), the learned interaction patterns are generalized to unseen but semantically related relationships during inference. We validate BCTR on two SGG datasets: Visual Genome and Open Image V6. Results show that BCTR achieves superior performance compared to existing methods. Our contributions are summarized as follows:

- We propose a novel bidirectional conditioning factorization within a semantic-aligned space for SGG, enhancing information exchange between predicates and entities by introducing mutual dependence.
- We develop an end-to-end SGG model BCTR to implement our factorization. Specifically, BCG is designed to augment the feature spaces through bidirectional attention mechanisms, while RFA is introduced to regularize the feature space with VLPMs for facilitating BCG learning interaction patterns effectively.
- Extensive experiments on the Visual Genome and Open Image V6 datasets demonstrate that BCTR achieves state-of-the-art performance compared to baselines.

2. Related Work

Conditional Dependencies in One-stage SGG Inspired by one-stage detection methods [1, 27], previous studies have designed Relation Affinity Fields [23] or used query-based detection [30] for one-stage SGG. However, these methods perform poorly as they do not utilize entity detection information [18]. Recent works [4, 9, 26] have incorporated entity features to improve relationship detection. Nonetheless, these methods either condition predicates on entities [18, 26] or condition entities on predicates [6], resulting in unidirectional dependencies that limit feature interaction and thus restrict performance gains. Khandelwal et al. [12] argue that SGG can benefit from dynamic conditioning on the image. However, their predicate remains unidirectionally conditioned on the entity, and performance improvement relies on the loss function rather than network architecture. In contrast, our proposed BCG introduces internal bidirectional dependencies, iteratively enhancing features in each round. Additionally, the RFA module enables BCG to learn feature interactions within a semantic-aligned space, improving the generalization of learned interaction patterns to semantically related relationships.

Message Passing in SGG Message passing aims to boost SGG performance through interactions between predictions and their context. Zhu et al. [38] categorize it into local (within a triplet) and global (across all elements) message passing. They observe that prediction structures influence the types of message passing: triplet set-based methods [20] utilize local message passing, while chain [31], tree [28], and fully-connected graph [17] structures enable global message passing. Global message passing mitigates local ambiguities by integrating contextual information. In contrast to previous methods, we design the BiAtt-based BCG to achieve global message passing within a set structure, leveraging implicit global connections for more efficient information exchange.

External Knowledge in SGG Enhancing scene graph generation with external knowledge is a vital research direction [38]. Previous approaches [14, 33] typically extract statistical information from textual sources like Wikipedia, but such data often fails to capture the complex patterns of commonsense, leading to limited learning improvements [21]. Gu et al. [7] propose a knowledge-based module that refines features by reasoning over a collection of commonsense knowledge retrieved from ConceptNet. However, Zareian et

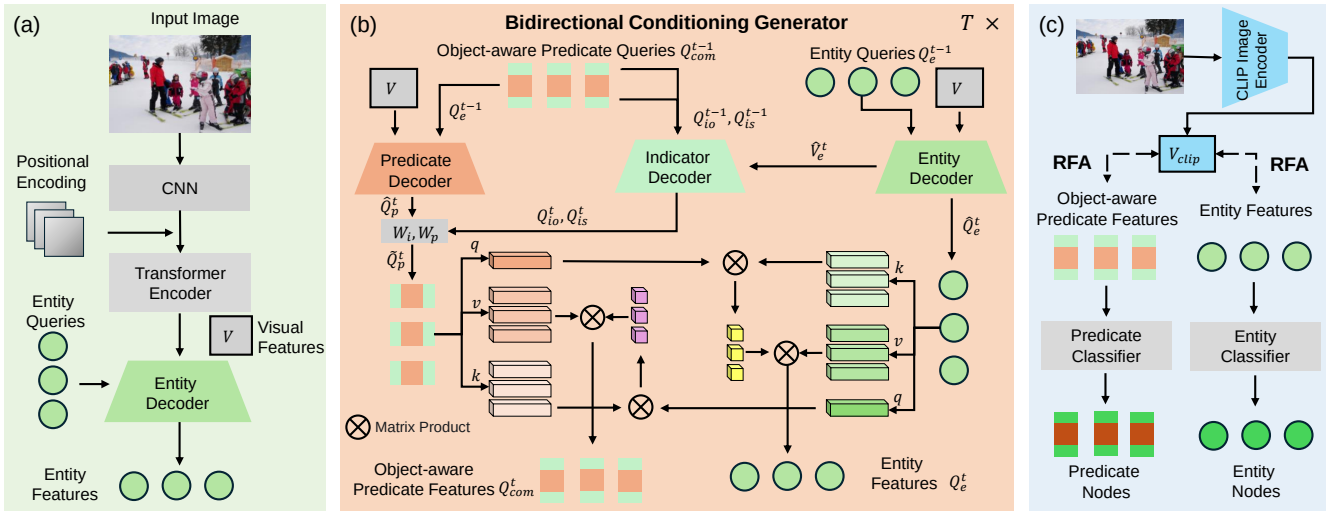

Figure 2. **Overview of the BCTR.** (a) Visual and entity features are extracted from the input image. (b) The compositional predicate and entity queries are iteratively updated through the proposed BCG. (c) During training, the output features from various decoders are regularized by the RFA. Final predictions are generated from these distilled features.

al. [34] noted that incomplete and inaccurate commonsense can hinder task performance. In contrast, BCTR leverages visual-language pre-trained models as a source of external knowledge. By embedding this knowledge through feature distillation, our model learns richer feature representations for scene graph generation, achieving superior performance on complex and unseen relationships.

3. Problem Formulation

SGG aims to detect objects and predicates in the input image and represent them as a scene graph $\mathcal{G} = \{\mathcal{V}, \mathcal{E}\}$, where $\mathcal{V}$ and $\mathcal{E}$ denote the sets of vertices and edges, respectively. $\mathcal{V}$ represents all detected objects in the image, while $\mathcal{E}$ comprises the predicates between object pairs. The categories of objects and predicates are defined by the dataset.

Previous one-stage SGG methods typically assume a unidirectional information flow, such as $I \rightarrow s, o \rightarrow p$ [4], or $I \rightarrow p \rightarrow s, o$ [6], limiting mutual benefits between the two predictions. I, o, s, and p are the abbreviation of the image, object, subject and predicate, respectively. Teng et al. [30] formulate SGG as $I \rightarrow p, s, o$ to facilitate feature interaction. However, optimizing over the massive compositional triplet space is challenging. This paper proposes a novel factorization for SGG, as shown in Eq. 1.

$$Pr(E, P|I) = Pr(\hat{E}, \widetilde{P}|I) \cdot Pr(E, P|\hat{E}, \widetilde{P}). \quad (1)$$

where E and P represent the entity and predicate estimates, respectively. The first term reflects $I \rightarrow s, o$ and $I \rightarrow p$, avoiding the optimization issues caused by the large compositional space. The second term enforces bidirectional dependencies $p \leftrightarrow s, o$, allowing the two predictions to benefit from each other.

After acquiring the predictions of entities and predicates, we formulate SGG as a bipartite graph construction task based on previous work [18]. Specifically, the predictions of entities and predicates from image form two node sets $\mathcal{V}_e$ and $\mathcal{V}_p$, respectively. Two directional edge sets $\mathcal{E}_{ep}$ and $\mathcal{E}_{pe}$ are used to connect these node sets, representing the connections from entities to predicates and vice versa. The bipartite graph is then represented as $\mathcal{G}_b = \{\mathcal{V}_e, \mathcal{V}_p, \mathcal{E}_{ep}, \mathcal{E}_{pe}\}$, from which the scene graph of the image can be extracted.

4. Method

This section presents BCTR for implementing the factorization in Eq. 1. The overview of BCTR is shown in Fig. 2, which comprises two main modules: BCG and RFA. We detail these components in the sequel.

4.1. Feature Extraction

Inspired by the previous one-stage detection method DETR [1], we utilize a CNN and Transformer to extract features $V \in \mathbb{R}^{w \times h \times c}$ from the input image I, where w, h, and c represent the width, height, and feature channels, respectively. Since previous one-stage SGG methods have shown that models struggle to capture predicates directly from image features without using intermediate information (e.g., entity features), we further extract entity features $V_e \in \mathbb{R}^{N_e \times c}$ from image feature V as auxiliary features, as shown in the following:

$$V_e = f_e(V, Q_e), \quad (2)$$

where $f_e, Q_e \in \mathbb{R}^{N_e \times c}$ represent the transformer-based decoder and the learnable queries, respectively, where N_e denoting the number of queries.

4.2. Bidirectional Conditioning Generator

This subsection details the Bidirectional Conditioning Generator, as shown in Fig. 2. BCG comprises two interactive branches that take visual features V as input and output augmented entity features and compositional predicate features, respectively. To improve performance, we introduce the iterative improvement mechanism into BCG. Specifically, we factorize the conditional distribution of entity and predicate according to Eq. 1, which are as follows:

$$Pr(E^t|I, E^{t-1}, \widetilde{P}^t) = Pr(\hat{E}^t|I, E^{t-1}) \cdot Pr(E^t|\hat{E}^t, \widetilde{P}^t), \quad (3)$$

$$Pr(P^t|I, P^{t-1}, \hat{E}^t) = Pr(\widetilde{P}^t|I, P^{t-1}, \hat{E}^t) \cdot Pr(P^t|\hat{E}^t, \widetilde{P}^t), \quad (4)$$

where E^t and P^t represent the entity and predicate estimates at phase t, respectively, while $\widetilde{}$ and $\hat{}$ denote the intermediate estimates at each phase. The first terms of the two equations predict the intermediate estimates $\widetilde{P}^t$ and $\hat{E}^t$ based on the previous estimates and the image, corresponding to the first term of Eq. 1. The second terms establish bidirectional dependencies between entities and predicates, corresponding to the second term of Eq. 1. At each phase t, these estimates will be updated through the corresponding decoder layer. The implementation details of Eq. 3 and Eq. 4 are introduced as follows.

Inspired by previous work [18], we initialize Q_p^0 randomly to generate the compositional predicate queries Q_{com}^{t-1} for the current scene, implemented as follows:

$$Q_{com}^{t-1} = A(q = Q_p^0, k = V_e, v = V_e), \quad (5)$$

where A denotes the attention block, and q, k, v represent the query, key, and value of the attention network, respectively. Q_{com}^{t-1} serves as the input to the predicate branch at phase t, consisting of three sub-queries: Q_{io}^{t-1}, Q_p^{t-1}, and Q_{is}^{t-1}. Q_e^{t-1} is the input to the entity branch at phase t, initialized from V_e. At step t, Q_p^{t-1} and Q_e^{t-1} are updated with V via a cross-attention module, defined as follows:

$$\hat{Q}_e^t = A(q = Q_e^{t-1}, k = V, v = V), \quad (6)$$

$$\hat{Q}_p^t = A(q = Q_p^{t-1}, k = V, v = V). \quad (7)$$

The Eq. 6 corresponds to the first term of Eq. 3. Then, Q_{io}^{t-1} and Q_{is}^{t-1} are updated with entity features $\hat{Q}_e^t$ through cross-attention. This step aims to identify entity pairs that match the corresponding predicates from the current entity detection. The process is implemented as follows:

$$Q_{io}^t = A(q = Q_{io}^{t-1}, k = \hat{V}_e^t, v = \hat{V}_e^t), \quad (8)$$

$$Q_{is}^t = A(q = Q_{is}^{t-1}, k = \hat{V}_e^t, v = \hat{V}_e^t), \quad (9)$$

where $\hat{V}_e^t = V_e + \lambda\,\mathrm{Norm}(\hat{Q}_e^t)$. After updating these queries with the corresponding decoder, $\hat{Q}_p^t$ is further augmented with the updated indicator queries to adjust the predicate distribution, computed as follows:

$$\widetilde{Q}_p^t = (\hat{Q}_p^t + (Q_{io}^t + Q_{is}^t) \cdot W_i) \cdot W_p. \quad (10)$$

Eq. 7 to Eq. 10 correspond to the first term of Eq. 4, where W_i and W_p represent transformation matrices. The indicator queries Q_{io}^t and Q_{is}^t are computed from entity features, enhancing the predicate query $\widetilde{Q}_p^t$ based on current entity detections. However, entity detection does not yet leverage information from predicates. To address this, we introduce a bidirectional attention module to establish conditional dependencies between entities and predicates, enabling mutual augmentation of entity and predicate features. This module is implemented as follows:

$$Q_e^t = A(q = \hat{Q}_e^t, k = \widetilde{Q}_p^t, v = \widetilde{Q}_p^t), \quad (11)$$

$$Q_p^t = A(q = \widetilde{Q}_p^t, k = \hat{Q}_e^t, v = \hat{Q}_e^t). \quad (12)$$

Eq. 11 and Eq. 12 correspond to the second terms of Eq. 3 and Eq. 4, respectively. After the bidirectional interaction, the updated queries Q_p^t, Q_{io}^t, Q_{is}^t and Q_e^t are used as inputs for the next phase. Through multi-stage iterative refinement, the bidirectional interaction between entities and predicates is progressively enhanced. At the end of the iterations, the final queries Q_{com}^{end} and Q_e^{end} are fed into the corresponding Multi-Layer Perceptrons (MLPs) to predict the entity and predicate distributions, respectively.

4.3. Random Feature Alignment

In this subsection, we introduce the details of Random Feature Alignment, illustrated in Fig. 3. RFA distills knowledge from a pre-train CLIP model, constraining the feature space of various decoders aligned with CLIP. Furthermore, the parameters of the predicate and entity classifiers are initialized with the CLIP text encoder and fine-tuned on the SGG dataset. The specifics of feature distillation and classifier initialization are detailed as follows.

Random Feature Alignment As illustrated in Fig. 1 (a), the class imbalance in SGG datasets makes it challenging for BCG to capture feature interaction patterns for tail relationships from rare samples during training. Additionally, the learned feature interactions perform poorly on unseen relationships during inference. To address these issues, we propose RFA, which aligns the SGG feature space with that of a pre-trained vision-language model. In this semantically aligned feature space, BCG can effectively learn feature interaction patterns during training, and the learned patterns generalize better to unseen relationships.

Specifically, the input image is fed into the CLIP visual encoder to obtain V_{clip}. Since CLIP is trained with image captions, the encoder features V_{clip} are inclined to capture the gist of the image. However, images often contain multiple relationships. Simply aligning the decoder's features

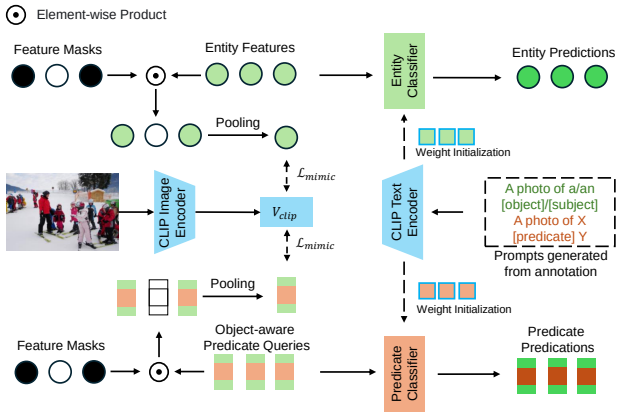

Figure 3. Random Feature Alignment for the entity and predicate prediction. First, the decoder features are randomly distilled with CLIP features. Then, the classifier weights are initialized with vectors generated by the CLIP text decoder, which encodes the ground-truth labels. This alignment ensures that the visual features can be accurately classified.

Q_p^{end} and Q_e^{end} with the CLIP feature V_{clip} may compromise the feature diversity of SGG. To preserve this diversity, we randomly select a subset of the decoder's features before each alignment, ensuring that the distilled features retain diversity while being aligned with CLIP. The overall masked distillation process is as follows:

$$\mathcal{L}_{mimic} = \left|V_{clip} - \frac{1}{N_p}\sum_{i=1}^{N_p} \bar{Q}_p^{end}\right| + \left|V_{clip} - \frac{1}{N_e}\sum_{i=1}^{N_e} \bar{Q}_e^{end}\right|, \quad (13)$$

where $\bar{Q}_p^{\text{end}}$ and $\bar{Q}_e^{\text{end}}$ are randomly sampled from Q_p^{end} and Q_e^{end}, respectively. N_p and N_e denote the numbers of predicate and entity queries. An example is shown in Fig. 3. Taking $Q_p^{\text{end}} \in \mathbb{R}^{N_e \times c}$ as an example, the mask vectors $V_{\text{mask}} \in \mathbb{R}^{N_e \times 1}$ are generated with a mask ratio α. The values of V_{mask} are set to 0 with probability α, and the remaining values are set to $(1/(1-\alpha))$. Then, the dimensions of V_{mask} are expanded and multiplied with Q_p^{end} to produce $\bar{Q}_e^{\text{end}}$. Finally, the mean feature of $\bar{Q}_e^{\text{end}}$ is used to match the pre-trained features, as described in Eq. 13.

Through random sampling features, some features are aligned with CLIP features, while others capture content that may be missing from CLIP features. After training, the feature space of the decoders aligns with CLIP's feature space, enabling multiple queries to capture the rich triplet relationships within the image.

CLIP-based Classifier After feature distillation, the decoder features Q_p^{end} and Q_e^{end} are aligned with CLIP. To effectively utilize these features, we introduce classifiers based on CLIP text features. Specifically, we generate descriptions by replacing $*$ in templates like "A photo of a/an *" or "A photo of X * Y" with the corresponding entity and predicate classes from the target dataset. These descriptions are input to the CLIP text encoder to obtain the corresponding feature vectors W_{ent} and W_{pre}. The resulting vectors are then used to initialize the parameters of the entity and predicate classifiers. Through the classifier layer, the decoder features Q_p^{end} and Q_e^{end} are used to calculate their cosine similarity with each category, and probabilities are derived from these similarity scores. During training, both classifiers are fine-tuned with a smaller learning rate to improve performance on the SGG datasets. The entire process is illustrated in Fig. 3.

4.4. Graph Assembling

Inspired by previous work [18], this section elaborates on the process of combining predicted entity and object-aware predicate nodes to generate triplets. Taking the connection between objects and predicates as an example, given the object node set N_o and the predicate node set N_p, we first construct the adjacency matrix M_o, which represents the distance between these nodes. The calculation is as follows:

$$M_o = d_{loc}(B_o, B_{po}) \cdot d_{cls}(P_o, P_{po}), \quad (14)$$

where d_{loc} and d_{cls} are distance functions used to measure matching quality in terms of bounding box locations and classes. Specifically, B_o, B_{po}, P_o, and P_{po} represent the bounding box predictions and classification distributions for objects and the indicators, respectively. Similarly, the adjacency matrix M_s between objects and predicates is calculated in the same way. By selecting the top K relationships from the two adjacency matrices M_s and M_o, the final predictions are obtained in the form $T = \{(B_o, B_s, B_p, P_o, P_s, P_p)\}$. Additional details on graph generation are provided in the supplementary materials.

4.5. Training and Inference

Training To optimize the parameters of the proposed model, we design a multi-task loss function consisting of three components: L_{ent} for the loss for entity prediction, L_{pre} for predicate prediction, and L_{mimic} for feature distillation. The overall loss function is defined as follows:

$$\mathcal{L} = \mathcal{L}_{ent} + \mathcal{L}_{pre} + \mathcal{L}_{mimic}. \quad (15)$$

Since the entity detector follows a DETR-like architecture, $\mathcal{L}_{ent}$ takes a similar form as described in [1]. To calculate $\mathcal{L}_{pre}$, we first convert the ground-truth relationships in the image into the same format as predictions T, denoted as T_{gt}. Then, the Hungarian matching algorithm is used to measure the cost between the ground truth and predictions, incorporating both predicate and entity information. The cost is computed as follows:

$$C = \lambda_p C_p + \lambda_e C_e, \quad (16)$$

where C_p and C_e represent the costs for the predicate and entity, respectively. The matching results are obtained by

Table 1. The Results Comparison in Visual Genome

Method		mR@			R@			mR@100		
		20	**50**	**100**	**20**	**50**	**100**	**Head**	**Body**	**Tail**
Two-stage	MOTIFS [35]	4.2	5.7	-	21.4	27.2	-	-	-	-
	RelDN [36]	-	6.0	7.3	-	31.4	35.9	-	-	-
	VCTree-TDE [29]	-	9.3	11.1	-	19.4	23.2	-	-	-
	BGNN [17]	7.5	10.7	12.6	23.3	31.0	35.8	**34.0**	12.9	6.0
	RepSGG [22]	6.7	9.3	11.4	22.5	29.6	34.8	31.3	11.2	5.3
One-stage	FCSGG [23]	2.7	3.6	4.2	16.1	21.3	25.1	-	-	-
	SRCNN [30]	6.2	8.6	10.3	**26.1**	**33.5**	**38.4**	-	-	-
	ISGG [12]	-	8.0	8.8	-	29.7	32.1	31.7	9.0	1.4
	Relationformer [26]	4.6	9.3	10.7	22.2	28.4	31.3	-	-	-
	SGTR [18]	-	12.0	15.2	-	24.6	28.4	28.2	18.6	7.1
	RelTR [4]	6.8	10.8	12.6	21.2	27.5	-	30.6	14.4	5.0
	SG2HOI [9]	**8.9**	11.4	13.9	21.2	25.9	30.3	27.5	18.2	5.3
	DSGG [8]	-	13.0	17.3	-	32.9	38.5	-	-	-
	EGTR [10]	5.5	7.9	10.1	23.5	30.2	34.3	-	-	-
	PGSG [19]	-	10.5	12.7	-	20.3	23.6	-	-	-
	BCTR (ours)	8.1	**13.7**	**18.4**	20.1	24.8	27.7	27.7	**22.0**	**11.9**
One-stage with statistical-based long-tail strategy	ISGG+Rw [12]	-	15.7	17.8	-	**27.2**	**29.8**	**28.5**	18.8	13.3
	SGTR+Bilvl [18]	-	15.8	20.1	-	20.6	25.0	21.7	21.6	17.1
	RelTR+LA [4]	9.7	14.2	-	**19.8**	25.9	-	28.3	19.4	10.2
	BCTR (ours)+LA	**12.7**	**17.4**	**20.9**	17.2	21.9	25.2	24.6	**23.4**	**17.4**

selecting the minimum costs and are used to guide the calculation of $\mathcal{L}_{pre}$. Specifically, $\mathcal{L}_{pre}$ consists of two parts: $\mathcal{L}^{i}_{pre}$ and $\mathcal{L}^{p}_{pre}$, representing the losses for indicator and predicate, respectively. Both $\mathcal{L}^{i}_{pre}$ and $\mathcal{L}^{p}_{pre}$ include losses for bounding box predictions $\mathcal{L}_{box}$ (GIOU loss) and classification distributions $\mathcal{L}_{cls}$ (cross-entropy loss). The feature distillation loss $\mathcal{L}_{mimic}$ is implemented using the L1 loss.

Inference During inference, the feature distillation module is removed, as it is only used during training. After constructing the graph with predictions, we obtain $K \cdot N_p$ triplets. To produce the final results, we first filter out self-connected predictions where the object and subject in a triplet are identical. Next, we re-rank all triplets based on a belief score S and select the top K as the final prediction results. The belief score S is calculated as the product of the classification probabilities of the corresponding subject entity, object entity, and predicate.

5. Experiments

Datasets We conduct evaluation experiments on two representative scene graph generation datasets, namely Visual Genome [15] and Open Image V6 [16].

Evaluation Metrics The evaluation metrics follow previous works [28]. For Visual Genome, mean Recall (mR@) represents the average recall across all classes, while Recall (R@) reflects the model's overall recall performance across categories. Additionally, we report mR@100 for each category group (head, body, and tail) to assess the model's performance on long-tail distributions. For Open Images V6, in addition to R@ and mR@, we use weighted metrics $wmAP_{phr}$, $wmAP_{rel}$ and $score_{wtd}$) to provide a more class-balanced evaluation.

Implementation Details We use ResNet-101 and DETR as the image feature extraction modules. The entity decoder adopts the same architecture as the DETR decoder. The numbers of entity and predicate queries are set to 100 and 160, respectively, and the number of iterations (stages) is empirically set to 6. To ensure training convergence, we begin by training the entity decoder on the dataset with the entity feature distillation loss as defined in Eq. 13. Next, we train the entire model with feature distillation on the dataset, keeping the entity decoder frozen. Finally, we unfreeze the entity decoder and activate bidirectional attention for joint training. Feature distillation losses are calculated for the entity and decoder after BCG. Furthermore, to ensure that BCG's feature interaction performs in a semantically aligned space, we also compute the entity distillation loss before BCG to enforce constraints on the feature space during joint learning. Additional details on parameter settings are provided in the supplementary materials.

Table 2. The Results Comparison in Open Image V6

Method	mR@ 50	R@ 50	wmAP rel	wmAP phr	score
HOTR [13]	40.1	52.7	19.4	21.5	26.9
AS-Net [3]	35.2	55.3	25.9	27.5	32.4
SGTR(Li et al. 2022)	42.6	59.9	**37.0**	38.7	42.3
PGTR [19]	40.7	62.0	22.7	28.0	30.8
BCTR (ours)	**48.8**	**68.6**	36.0	**39.0**	**42.5**

Table 3. Ablation Study on Model Components

BCG	RFA	mR@20/50/100	R@20/50/100	H/B/T
✗	✗	7.4/12.8/17.0	19.6/24.2/27.3	26.9/21.3/9.7
✓	✗	7.7/13.2/17.6	19.9/24.6/27.6	27.2/21.5/10.9
✗	✓	7.9/13.2/17.9	**20.4/25.1/28.2**	**28.1/22.4**/10.5
✓	✓	**8.1/13.7/18.4**	20.1/24.8/27.7	27.7/22.0/**11.9**

5.1. Comparisons with State-of-the-Art Methods

Baselines Since BCTR is a one-stage scene graph generation method, we primarily compare it with other current one-stage SGG methods, which are mainly transformer-based [4, 9, 12, 18, 26]. Additionally, we compare our method with several representative two-stage methods [17, 29, 35, 36]. Although existing one-stage methods do not specifically tackle the long-tail problem, previous studies have reported results using statistical-based unbiased training (e.g., bi-level sampling [17]) or inference (e.g., logit adjustment [24]) techniques. For further comparison, we also report our method's performance with these statistical-based unbiased approaches.

Results of Visual Genome The results in Tab. 1 demonstrate that BCTR outperforms other baselines in mR@ performance. By leveraging BCG and RFA, BCTR learns balanced feature representations for SGG, achieving a notable improvement of 14% and 21% in mR@K over state-of-the-art methods, indicating enhanced recall across various categories. In particular, BCTR excels in the body and tail categories, exceeding the second-best method by 18% and 67%, respectively. This performance is attributed to RFA, which constrains the feature space, enabling BCG to capture generalizable feature interactions even from rare samples, thereby boosting tail-category performance.

Our R@K is lower because R@K and mR@K emphasize different performance aspects. Given the imbalanced VG dataset, R@K focuses on head predicates with abundant samples, while mR@K better reflects tail predicates, making it a fairer metric for long-tail datasets by minimizing the influence of dominant relationships [2, 5, 17]. Additionally, our DETR-based detector struggles with small entities common in the VG dataset [18], which contributes to the lower R@K. Improving small-object detection would enhance R@K. Experimental results in Tab. 1 further confirm that, when combined with statistical long-tail strategies, BCTR surpasses other methods in the body and tail categories and significantly improves mR@ performance.

Table 4. Ablation Study on Feature Interactions

Method	mR@20/50/100	R@20/50/100	H/B/T
BCG-UniAtt	7.6/13.1/17.5	19.6/24.2/27.3	27.0/21.3/10.8
BCG-BiAtt	**7.7/13.2/17.6**	**19.9/24.6/27.6**	**27.2/21.5/10.9**

Table 5. Ablation Study on Distillation Strategy

Method	mR@20/50/100	R@20/50/100	H/B/T
TC	7.8/13.0/17.8	20.1/25.1/**28.3**	28.2/22.4/10.0
TC-RFA	**7.8/13.3/18.2**	**20.4**/25.1/28.2	28.1/**22.5/10.9**
LP	7.5/13.0/17.2	20.1/**25.3**/28.7	**28.4**/22.2/8.9
LP-RFA	7.5/13.0/17.6	20.2/25.2/28.3/	28.0/21.9/10.2

Results of Open Image V6 The results of Open Image V6 are presented in Tab. 2. These experimental results demonstrate that our approach has significantly enhanced the recall performance of SGG while achieving superior or comparable weighted mAP metrics. Notably, mR@50 has improved by 6.19, demonstrating that the SGG tasks benefit from the proposed bidirectional conditioning and random feature alignment.

5.2. Ablation Studies

Model Components The results of the ablation study on model components are presented in Tab. 3, showing the performance of four model variants obtained by combining BCG and RFA. In Tab. 3, models with BCG include two additional decoder layers (i.e., bidirectional attention layers) compared to models without BCG. For fair comparison, we add two extra decoder layers to the predicate decoder in the models without BCG. The results demonstrate that both BCG and RFA contribute to improvements in mR@ and R@. Combining the two modules further improves recall in the tail category, resulting in a superior mR@100 performance of 18.4. We attribute this improvement to BCG's ability to learn better feature interactions within a semantically aligned space, which is regularized by RFA, thereby showing superior generalization to infrequent relationship combinations (i.e., tail categories). The ablation study indicates that BCG and RFA are highly compatible, and integrating the two modules further enhances performance on the scene graph generation task.

Feature Interaction Strategy We compare the performance of two different internal message interaction patterns: Unidirectional Attention (UniAtt) and Bidirectional Attention (BiAtt). In UniAtt, only predicate-to-entity attention is activated, while in BiAtt, both entity-to-predicate and predicate-to-entity attention are enabled. The experimental results are reported in Tab. 4, where BiAtt demonstrates

Table 6. The Performance of Zero-shot Triplets Generation

Method	zR@50/100
BGNN [17]	0.4/0.9
VCTree-TDE [29]	2.6/3.2
SGTR [18]	2.4/5.8
ISGG [12]	3.9/5.6
SG2JOIT [9]	2.5/3.7
BCTR (ours) w/o BCG+RFA	3.6/5.1
BCTR (ours) w/ BCG	3.7/5.4
BCTR (ours) w/ RFA	4.1/6.0
BCTR (ours) w/ BCG+RFA	**4.4/6.2**

Table 7. Ablation Study on Mask Ratio

Mask Ratio	mR@20/50/100	R@20/50/100	H/B/T
0	7.8/13.0/17.8	20.1/**25.1/28.3**	**28.2**/22.4/10.0
0.25	7.8/13.2/17.8	20.2/24.9/27.9	27.8/22.5/10.2
0.5	**7.8/13.3/18.2**	**20.4**/25.1/28.2	28.1/**22.5/10.9**
0.75	7.5/13.3/17.9	20.2/24.8/28.0/	28.0/22.4/10.5

better performance than UniAtt, indicating the effectiveness of the designed Bidirectional Attention for the scene graph generation task.

Distillation strategy We conduct ablation experiments on distillation strategies to elucidate the effectiveness of the proposed RFA. The results are presented in Tab. 5, where Trainable Classifier (TC) and Learnable Prompt (LP) [37] represent two CLIP-based classifiers. The results indicate that Random Feature Alignment enhances the performance of both classifiers. We attribute this improvement to RFA's ability to align decoder features with CLIP, while enabling queries to capture additional objects and predicates in the image that may not be represented by CLIP. Furthermore, the results demonstrate that TC outperforms LP on scene graph generation task.

Zero-shot Recall The Zero-shot Recall (zR@) of the proposed model is reported in Tab. 6. zR@ measures the recall of triplets unseen during training, reflecting the model's generalization ability. The results show that Bidirectional Conditioning Generator provides a minor improvement in zR@, with zR@50/100 increasing by 0.1 and 0.3, respectively. When combined with Random Feature Alignment, zR@ significantly improves to 4.4 and 6.2, surpassing other baselines. This finding aligns with the observations in Tab. 3, suggesting that feature interactions learned in semantically aligned spaces generalize more effectively to unseen category relationships.

Mask Ratio We set α between 0 and 1 to evaluate how the mask ratio affects the model. The experimental results show high R@K values when α is close to 0, as the model captures the main content of the image after aligning with CLIP feature space, which accounts for a higher proportion

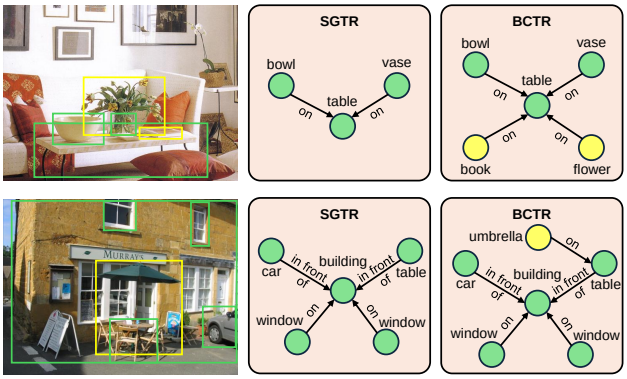

Figure 4. Qualitative results of our method and another method on the VG dataset. When leveraging identical DETR-based detectors, the bidirectional interaction mechanism of BCTR reduces missed detections (highlighted as yellow nodes) and enhances performance on SGG tasks.

of the VG dataset. As α increases, the model captures more diverse content, leading to improvements in mR@K. However, when α approaches 1, performance declines due to insufficient feature distillation.

Qualitative Analysis We visualize the detection results of the VG dataset in Fig. 4. For clarity, only the directed edges matching the ground-truth are shown. The experimental results indicate that, with identical DETR-based detectors, the bidirectional interaction mechanism in BCTR mutually enhances entity and predicate detection, leading to better performance on SGG compared to the baseline.

6. Conclusion

In this study, we propose a novel bidirectional conditioning factorization in semantic-aligned space for SGG and implement it by developing an end-to-end SGG model BCTR. BCTR enhances the performance of SGG tasks in two main aspects. First, the Bidirectional Conditioning Generator is designed to facilitate information interaction between entity and predicate predictions through internal bidirectional conditioning and external iterations. Second, Random Feature Alignment is introduced to facilitate BCG learning interaction patterns by randomly aligning the feature space with a pre-trained visual language model, improving generalization for semantically related relationships during inference. We perform experiments on several datasets: Visual Genome and Open Images V6, and the results demonstrate that our method achieves state-of-the-art performance.

Potential Limitation. The main limitation of the proposed method is the ongoing challenge of distilling features from VLPMs to SGG. Although RFA helps bridge the gap between CLIP's focus on global features and SGG's need for local predicates, further exploration of fine-grained VLPM enhancements could improve performance.

References

[1] Nicolas Carion, Francisco Massa, Gabriel Synnaeve, Nicolas Usunier, Alexander Kirillov, and Sergey Zagoruyko. End-to-end object detection with transformers. In *European conference on computer vision*, pages 213–229. Springer, 2020. 1, 2, 3, 5

[2] Xiaojun Chang, Pengzhen Ren, Pengfei Xu, Zhihui Li, Xiaojiang Chen, and Alex Hauptmann. A comprehensive survey of scene graphs: Generation and application. *IEEE Transactions on Pattern Analysis and Machine Intelligence*, 45(1): 1–26, 2021. 7

[3] Mingfei Chen, Yue Liao, Si Liu, Zhiyuan Chen, Fei Wang, and Chen Qian. Reformulating hoi detection as adaptive set prediction. In *Proceedings of the IEEE/CVF Conference on Computer Vision and Pattern Recognition*, pages 9004–9013, 2021. 7

[4] Yuren Cong, Michael Ying Yang, and Bodo Rosenhahn. Reltr: Relation transformer for scene graph generation. *IEEE Transactions on Pattern Analysis and Machine Intelligence*, 2023. 2, 3, 6, 7

[5] Alakh Desai, Tz-Ying Wu, Subarna Tripathi, and Nuno Vasconcelos. Learning of visual relations: The devil is in the tails. In *Proceedings of the IEEE/CVF International Conference on Computer Vision*, pages 15404–15413, 2021. 7

[6] Alakh Desai, Tz-Ying Wu, Subarna Tripathi, and Nuno Vasconcelos. Single-stage visual relationship learning using conditional queries. *Advances in Neural Information Processing Systems*, 35:13064–13077, 2022. 2, 3

[7] Jiuxiang Gu, Handong Zhao, Zhe Lin, Sheng Li, Jianfei Cai, and Mingyang Ling. Scene graph generation with external knowledge and image reconstruction. In *Proceedings of the IEEE/CVF conference on computer vision and pattern recognition*, pages 1969–1978, 2019. 2

[8] Zeeshan Hayder and Xuming He. Dsgg: Dense relation transformer for an end-to-end scene graph generation. In *Proceedings of the IEEE/CVF Conference on Computer Vision and Pattern Recognition*, pages 28317–28326, 2024. 6

[9] Tao He, Lianli Gao, Jingkuan Song, and Yuan-Fang Li. Toward a unified transformer-based framework for scene graph generation and human-object interaction detection. *IEEE Transactions on Image Processing*, 32:6274–6288, 2023. 2, 6, 7, 8

[10] Jinbae Im, JeongYeon Nam, Nokyung Park, Hyungmin Lee, and Seunghyun Park. Egtr: Extracting graph from transformer for scene graph generation. In *Proceedings of the IEEE/CVF Conference on Computer Vision and Pattern Recognition*, pages 24229–24238, 2024. 6

[11] Justin Johnson, Ranjay Krishna, Michael Stark, Li-Jia Li, David Shamma, Michael Bernstein, and Li Fei-Fei. Image retrieval using scene graphs. In *Proceedings of the IEEE conference on computer vision and pattern recognition*, pages 3668–3678, 2015. 1

[12] Siddhesh Khandelwal and Leonid Sigal. Iterative scene graph generation. *Advances in Neural Information Processing Systems*, 35:24295–24308, 2022. 2, 6, 7, 8

[13] Bumsoo Kim, Junhyun Lee, Jaewoo Kang, Eun-Sol Kim, and Hyunwoo J Kim. Hotr: End-to-end human-object interaction detection with transformers. In *Proceedings of the IEEE/CVF Conference on Computer Vision and Pattern Recognition*, pages 74–83, 2021. 7

[14] Hyeongjin Kim, Sangwon Kim, Dasom Ahn, Jong Taek Lee, and Byoung Chul Ko. Scene graph generation strategy with co-occurrence knowledge and learnable term frequency. *arXiv preprint arXiv:2405.12648*, 2024. 2

[15] Ranjay Krishna, Yuke Zhu, Oliver Groth, Justin Johnson, Kenji Hata, Joshua Kravitz, Stephanie Chen, Yannis Kalantidis, Li-Jia Li, David A Shamma, et al. Visual genome: Connecting language and vision using crowdsourced dense image annotations. *International journal of computer vision*, 123:32–73, 2017. 6

[16] Alina Kuznetsova, Hassan Rom, Neil Alldrin, Jasper Uijlings, Ivan Krasin, Jordi Pont-Tuset, Shahab Kamali, Stefan Popov, Matteo Malloci, Alexander Kolesnikov, et al. The open images dataset v4: Unified image classification, object detection, and visual relationship detection at scale. *International Journal of Computer Vision*, 128(7):1956–1981, 2020. 6

[17] Rongjie Li, Songyang Zhang, Bo Wan, and Xuming He. Bipartite graph network with adaptive message passing for unbiased scene graph generation. In *Proceedings of the IEEE/CVF Conference on Computer Vision and Pattern Recognition*, pages 11109–11119, 2021. 2, 6, 7, 8

[18] Rongjie Li, Songyang Zhang, and Xuming He. Sgtr: End-to-end scene graph generation with transformer. In *proceedings of the IEEE/CVF conference on computer vision and pattern recognition*, pages 19486–19496, 2022. 2, 3, 4, 5, 6, 7, 8

[19] Rongjie Li, Songyang Zhang, Dahua Lin, Kai Chen, and Xuming He. From pixels to graphs: Open-vocabulary scene graph generation with vision-language models. In *Proceedings of the IEEE/CVF Conference on Computer Vision and Pattern Recognition*, pages 28076–28086, 2024. 6, 7

[20] Yikang Li, Wanli Ouyang, Xiaogang Wang, and Xiao'ou Tang. Vip-cnn: Visual phrase guided convolutional neural network. In *Proceedings of the IEEE conference on computer vision and pattern recognition*, pages 1347–1356, 2017. 2

[21] Bingqian Lin, Yi Zhu, and Xiaodan Liang. Atom correlation based graph propagation for scene graph generation. *Pattern Recognition*, 122:108300, 2022. 2

[22] Hengyue Liu and Bir Bhanu. Repsgg: Novel representations of entities and relationships for scene graph generation. *IEEE Transactions on Pattern Analysis and Machine Intelligence*, 2024. 6

[23] Hengyue Liu, Ning Yan, Masood Mortazavi, and Bir Bhanu. Fully convolutional scene graph generation. In *Proceedings of the IEEE/CVF Conference on Computer Vision and Pattern Recognition*, pages 11546–11556, 2021. 1, 2, 6

[24] Aditya Krishna Menon, Sadeep Jayasumana, Ankit Singh Rawat, Himanshu Jain, Andreas Veit, and Sanjiv Kumar. Long-tail learning via logit adjustment. *arXiv preprint arXiv:2007.07314*, 2020. 7

[25] Jiaxin Shi, Hanwang Zhang, and Juanzi Li. Explainable and explicit visual reasoning over scene graphs. In *Proceedings of the IEEE/CVF conference on computer vision and pattern recognition*, pages 8376–8384, 2019. 1

[26] Suprosanna Shit, Rajat Koner, Bastian Wittmann, Johannes Paetzold, Ivan Ezhov, Hongwei Li, Jiazhen Pan, Sahand Sharifzadeh, Georgios Kaissis, Volker Tresp, et al. Relationformer: A unified framework for image-to-graph generation. In *European Conference on Computer Vision*, pages 422–439. Springer, 2022. 2, 6, 7

[27] Peize Sun, Rufeng Zhang, Yi Jiang, Tao Kong, Chenfeng Xu, Wei Zhan, Masayoshi Tomizuka, Lei Li, Zehuan Yuan, Changhu Wang, et al. Sparse r-cnn: End-to-end object detection with learnable proposals. In *Proceedings of the IEEE/CVF conference on computer vision and pattern recognition*, pages 14454–14463, 2021. 1, 2

[28] Kaihua Tang, Hanwang Zhang, Baoyuan Wu, Wenhan Luo, and Wei Liu. Learning to compose dynamic tree structures for visual contexts. In *Proceedings of the IEEE/CVF conference on computer vision and pattern recognition*, pages 6619–6628, 2019. 2, 6

[29] Kaihua Tang, Yulei Niu, Jianqiang Huang, Jiaxin Shi, and Hanwang Zhang. Unbiased scene graph generation from biased training. In *Proceedings of the IEEE/CVF conference on computer vision and pattern recognition*, pages 3716–3725, 2020. 6, 7, 8

[30] Yao Teng and Limin Wang. Structured sparse r-cnn for direct scene graph generation. In *Proceedings of the IEEE/CVF Conference on Computer Vision and Pattern Recognition*, pages 19437–19446, 2022. 1, 2, 3, 6

[31] Danfei Xu, Yuke Zhu, Christopher B Choy, and Li Fei-Fei. Scene graph generation by iterative message passing. In *Proceedings of the IEEE conference on computer vision and pattern recognition*, pages 5410–5419, 2017. 2

[32] Xu Yang, Kaihua Tang, Hanwang Zhang, and Jianfei Cai. Auto-encoding scene graphs for image captioning. In *Proceedings of the IEEE/CVF conference on computer vision and pattern recognition*, pages 10685–10694, 2019. 1

[33] Ruichi Yu, Ang Li, Vlad I Morariu, and Larry S Davis. Visual relationship detection with internal and external linguistic knowledge distillation. In *Proceedings of the IEEE international conference on computer vision*, pages 1974–1982, 2017. 2

[34] Alireza Zareian, Zhecan Wang, Haoxuan You, and Shih-Fu Chang. Learning visual commonsense for robust scene graph generation. In *Computer Vision–ECCV 2020: 16th European Conference, Glasgow, UK, August 23–28, 2020, Proceedings, Part XXIII 16*, pages 642–657. Springer, 2020. 3

[35] Rowan Zellers, Mark Yatskar, Sam Thomson, and Yejin Choi. Neural motifs: Scene graph parsing with global context. In *Proceedings of the IEEE conference on computer vision and pattern recognition*, pages 5831–5840, 2018. 6, 7

[36] Ji Zhang, Kevin J Shih, Ahmed Elgammal, Andrew Tao, and Bryan Catanzaro. Graphical contrastive losses for scene graph parsing. In *Proceedings of the IEEE/CVF Conference on Computer Vision and Pattern Recognition*, pages 11535–11543, 2019. 6, 7

[37] Kaiyang Zhou, Jingkang Yang, Chen Change Loy, and Ziwei Liu. Learning to prompt for vision-language models. *International Journal of Computer Vision*, 130(9):2337–2348, 2022. 8

[38] Guangming Zhu, Liang Zhang, Youliang Jiang, Yixuan Dang, Haoran Hou, Peiyi Shen, Mingtao Feng, Xia Zhao, Qiguang Miao, Syed Afaq Ali Shah, et al. Scene graph generation: A comprehensive survey. *arXiv preprint arXiv:2201.00443*, 2022. 2